Cationic Vacancies in Anatase (TiO 2): Synthesis, Defect Characterization, and Ion-Intercalation Properties

Damien Dambournet

To cite this version:

Damien Dambournet. Cationic Vacancies in Anatase (TiO 2): Synthesis, Defect Characterization, and Ion-Intercalation Properties. Accounts of Chemical Research, 2022, pp.acs.accounts.1c00728. 10.1021/acs.accounts.1c00728 . hal-03572314

HAL Id: hal-03572314
https://hal.sorbonne-universite.fr/hal-03572314v1

Submitted on 14 Feb 2022

Cationic Vacancies in Anatase (TiO_2): Synthesis, Defect Characterization and ion-intercalation properties

Damien Dambournet [a,b*]

[a] Sorbonne Université, CNRS, Physicochimie des Electrolytes et Nanosystèmes Interfaciaux, PHENIX, F-75005 Paris, France

[b] Réseau sur le Stockage Electrochimique de l’Energie (RS2E), FR CNRS 3459, 80039 Amiens Cedex, France

CONSPECTUS. As one of the most studied materials, researches on titanium dioxide (TiO_2) have flourished over the years owing to technological interests ranging from energy conversion and storage to medical implants and sensors, to name a few. In this scope, the development of synthesis routes enabling the stabilization of reactive surface structure has been largely investigated. Among these routes, solution-based synthesis has been utilized to tailor the material’s properties spanning its atomic structural arrangement, or morphological aspects. One of the most investigated methods to stabilize crystals with tailored facets relies on the use of fluoride-based precursors. Fluoride ions not only provide a driving force for the stabilization of metastable/reactive surface structures but also alter the reactivity of titanium molecular precursors and in turn the structural features of the stabilized crystals. Here, we review recent progresses in the synthesis of solution-based synthesis

of anatase (one of the polymorphs of TiO_2) employing fluoride-precursor with emphasize of how cationic vacancies are stabilized by a charge-compensating mechanism and the resulting structural features associated with these defects. Finally, we will discuss the ion-intercalation properties of these sites with respect to lithium and polyvalent-ion such as Mg^{2+} and Al^{3+}. We will discuss in more details the relevant parameters of the synthesis that allow controlling the phase composition with the co-existence of oxide, fluoride and hydroxide ions within the anatase framework. The mechanism of formation of defective anatase nanocrystals has highlighted a solid-state transformation mostly implying oxolation reaction (condensation of hydroxide ions) that results in a decrease of the vacancies content, which can be synthetically controlled. The investigation of local fluorine environments probed by solid-state ^{19}F NMR revealed up to three coordination modes with different number of coordinated Ti^{4+} and vacancies. It further revealed the occurrence of single and adjacent pair of vacancies. These different host sites including native interstitial (and single/paired vacancies) display different ion-intercalation properties. We notably discussed the influence of the local anionic environments of vacancies on the thermodynamic of intercalation properties. The selective intercalation of polyvalent cations such as Mg^{2+} and Al^{3+} further supports the beneficial uses of defect chemistry for developing post lithium-ion batteries. It is expected that the ability to characterize the local structure of defects is a key toward the design of unique, tailored-made materials.

KEY REFERENCES

- Li, W.; Corradini, D.; Body, M.; Legein, C.; Salanne, M.; Ma, J.; Chapman, K. W.; Chupas, P. J.; Rollet, A.-L.; Julien, C.; Zhagib, K.; Duttine, M.; Demourgues, A.; Groult, H.; Dambournet, D. High Substitution Rate in TiO_2 Anatase Nanoparticles with Cationic Vacancies for Fast Lithium Storage. *Chem. Mater.* **2015**, *27* (14), 5014–5019.[1] *First evidences for the stabilization of cationic vacancies through oxide sublattice substitution in anatase TiO_2 and associated impact on the lithium storage mechanism.*

- Li, W.; Body, M.; Legein, C.; Borkiewicz, O. J.; Dambournet, D. Atomic Insights into Nanoparticle Formation of Hydroxyfluorinated Anatase Featuring Titanium Vacancies. *Inorg. Chem.* **2016**, *55* (14), 7182–7187.[2] *This paper reports on the crystal phase formation mechanism of cation-deficient anatase evidencing a solid-state transformation of the anionic and cationic sublattices occurring during solvothermal synthesis.*

- Koketsu, T.; Ma, J.; Morgan, B. J.; Body, M.; Legein, C.; Dachraoui, W.; Giannini, M.; Demortière, A.; Salanne, M.; Dardoize, F.; Groult, H.; Borkiewicz, O. J.; Chapman, K. W.; Strasser, P.; Dambournet, D. Reversible Magnesium and Aluminium Ions Insertion in Cation-Deficient Anatase TiO_2.[3] *This paper first reports the use of cationic vacancies as a mean to unlock the electrochemical activity with respect to polyvalent ions insertion in anatase.*

- Legein, C.; Morgan, B. J.; Fayon, F.; Koketsu, T.; Ma, J.; Body, M.; Sarou-Kanian, V.; Wei, X.-K.; Heggen, M.; Borkiewicz, O. J.; Strasser, P.; Dambournet, D. Atomic Insights into Aluminium-Ion Insertion in Defective Anatase for Batteries. *Angew. Chem. Int. Ed.* **2020**, *59* (43), 19247–19253.[4] *This paper describes the complex* Al^{3+}*-ion storage mechanism in cation-deficient anatase highlighting the local distortion induced by* Al^{3+} *and the role of anionic environments of vacancy on ion-intercalation energies.*

1. INTRODUCTION

Intercalation or insertion solids are atomic structures capable of reversibly hosting ions/electrons without major structural disruption.[5] Intercalation processes involve vacant sites that are either originally present[6] or formed during a de-insertion reaction of alkali-ions[7] and/or transition metal (TM) migration[8] as is typically encountered in layered transition metal oxides. Cationic (TM or alkali-ions) vacancies are thus prominent species involved in redox intercalation mechanism eventually yielding long-range ordering[9] or local clustering[10]. Cationic (TM) vacancies can naturally occur in inorganic frameworks (for example, in the spinel Fe_2O_3, *i.e.*, $Fe_{2.66}\square_{0.33}O_4$, where $\square$ represents iron vacancy) or intentionally generated via controlled synthesis methods with the possibility to tailor the vacancy-cation ratio.[11] In an ideal crystal lattice, cationic vacancies are expected to be absent. However, synthesis routes, particularly solution-based chemistry, can potentially yield deviations from the ideal/expected phase composition resulting in the stabilization of cationic vacancies, which might impact the material's properties. It is therefore of paramount importance to connect the synthesis methodology with the phase composition. Furthermore, it is essential to identify the mechanism of vacancy-driven charge compensation as it allows identifying the structural features associated with the stabilization of these cationic vacancies. Such features include vacancies clustering, changes of the anionic coordination modes, bond lengths and the electronic structure.

In this account, we present the results obtained by our group on anatase TiO_2, one of the polymorphs of titanium dioxide, and discuss the above-mentioned points related to the connection between the synthesis and the phase composition, the structural features of cation-deficient anatase and the resulting ion-intercalation properties. For this purpose, we recall that the anatase crystal lattice is built from edge-sharing TiO_6 octahedra connectivity. The framework exhibits interstitial sites capable of reversibly hosting Li^+ and Na^+ ions **(Figure 1)**.[12–14]

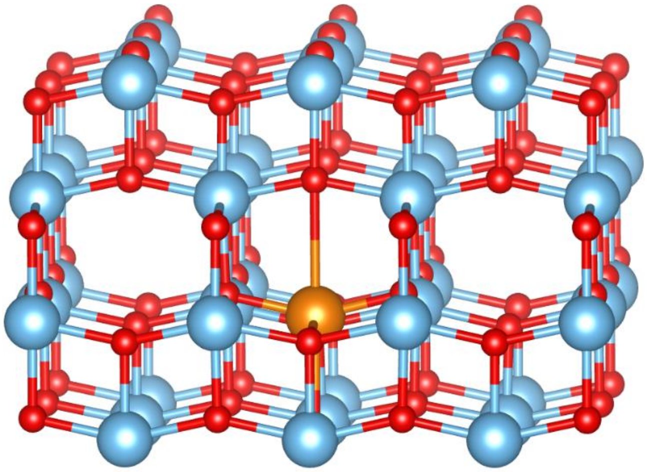

Figure 1. Structural representation of the anatase framework. The blue and red spheres represent Ti and O atoms, respectively. The orange sphere represents an ion intercalated in a native octahedral interstitial site.

2. SYNTHESIS ASPECTS AND COMPOSITIONAL/STRUCTURAL FEATURES

2.1. Synthesis parameters and phase composition

In the seminal work of Yang et *al*[15], micrometer anatase faceted single crystals with 47% of (001) surface were obtained using hydrothermal synthesis (aqueous solution of TiF_4, T=180 °C) with hydrofluoric acid as a morphology controlling agent. By using first-principles calculations, it has been concluded that fluoride-adsorbed (001) surfaces were more stable than the (101) one, providing a new route to control the crystal morphology of anatase. This work has stimulated intense research activities focusing on the amplified reactivity of the exposed (001) surface for different applications.[16] Hydro/solvothermal syntheses have been commonly employed with fluoride-based precursors to direct the growth of the metastable (001) surface at the expense of the thermodynamically stable (101)-type surface.[17] Note that fluoride ion is also know to act as a structure-directing agent favoring non-linear arrangements as found in anatase as opposed to linear arrangements displayed by the rutile structure.[18]

Following the intense researches devoted to the synthesis of faceted crystals of anatase, we posed the question about the phase composition of the obtained compounds. In particular, the presence of fluoride ions within the crystal lattice has been poorly investigated either because the synthetized compounds were subjected to post-treatments (heating or treated with a basic solution) to obtain pure TiO_2 and/or because of the use of inadequate characterization tools such as surface sensitive X-ray photoelectron spectroscopy and X-ray diffraction patterns typically indexed with anatase "TiO_2". Going back to the synthesis protocols typically employed in the literature[17], one can highlight the use of H_2O/organic solvents, aqueous HF, with Ti precursors such as TiF_4 and Ti-alkoxide. General considerations on the synthesis emphasize competitive reactions with respect to molecular Ti-precursor bonds, notably hydrolysis[19] and fluorolysis[20,21], which can be explained through similar nucleophilic characters[19] of HF and H_2O (the partial charge $\delta(F) = -0.42$ in HF and

$\delta(O) = -0.42$ in H_2O). Consequently, hydrolysis and fluorolysis reactions of the Ti-OR (R = alkyl groups) bonds can occur in the synthesis medium according to:

$$Ti - OR + H_2O \ \rightarrow Ti - OH + ROH$$

$$Ti - OR + HF \ \rightarrow Ti - F + ROH$$

Therefore, to address the question of whether the phase composition of the materials synthetized in the above-mentioned conditions might be different from titanium dioxide composition, we used a solvothermal synthesis employing Ti-alkoxyde, isopropanol and aqueous HF (the HF/Ti molar ratio was fixed to 2).[1] The reaction mixture was solvothermally treated at 90 °C for 12h resulting in the formation of a precipitate made of nanoparticles. Using this protocol, we demonstrated that indeed the phase composition largely deviated from the expected titanium dioxide. To characterize such deviation, we established a general phase composition where O^{2-} ions can be substituted by monovalent ions such as F^- and OH^-. Such anionic substitutions induce a charge-compensating mechanism yielding the stabilization of cationic vacancies according to $Ti_{1-x-y}\square_{x+y}O_{2-4(x+y)}F_{4x}(OH)_{4y}$, where □ represents a cationic vacancy.[1] This charge-compensating mechanism can be visualized in **Figure 2a**, which shows a structural representation of an anatase framework where $4O^{2-}$ ions are substituted by $4F^-$ accompanied with the stabilization of one vacancy. The phase composition was established by physical and analytical characterizations.[1] The presence of cationic vacancies was observed by using aberration-corrected transmission electron microscopy **(Figure 2b)** through variation in atomic column intensities which corresponds to a variation in the Ti atomic occupancy (see colored version of the TEM image).[3] Their quantification was assessed by real space refinement of the X-ray pair distribution function (PDF) data. Solid-state ^{19}F NMR unambiguously revealed the presence of fluoride ions within the anatase framework and further enabled its quantification. Finally, hydroxide ions were characterized by thermal analysis, ^{1}H NMR (see section 2.2) and their quantification deduced by electroneutrality following the general phase composition $Ti_{1-x-y}\square_{x+y}O_{2-4(x+y)}F_{4x}(OH)_{4y}$. The deduced phase composition was $Ti_{0.78}\square_{0.22}O_{1.12}F_{0.40}(OH)_{0.48}$.

To better understand the stabilization of such phase composition, we investigated the crystal formation mechanism by employing a time-dependent study allowing to capture the structural and compositional changes during the solvothermal synthesis.[2] In particular, we monitored the evolution of the vacancy content and the X-ray PDF coherent length during the course of the reaction **(Figure 2c)**. The results highlighted the formation of a highly defective phase at the early stage of the synthesis followed by a continuous decrease of the vacancy content. To understand such evolution, we evaluated the phase composition at the different stages of the synthesis and determined the relative proportion of anions in the anatase phase **(Figure 2d)**. The evolution demonstrated (i) at the early stage of the synthesis, the stabilization of highly defective anatase framework featuring a hydroxide-rich composition (free of O^{2-} ions) and (ii) a progressive decrease of the vacancies due to the partial dehydroxylation of the network forming oxide ions (oxolation reactions). The latter step was assigned to a solid-state transformation mechanism occurring at the particle level and not through a dissolution-recrystallization process. Remarkably, the content of fluoride ions remains relatively stable over the course of the reaction **(Figure 2d)**.

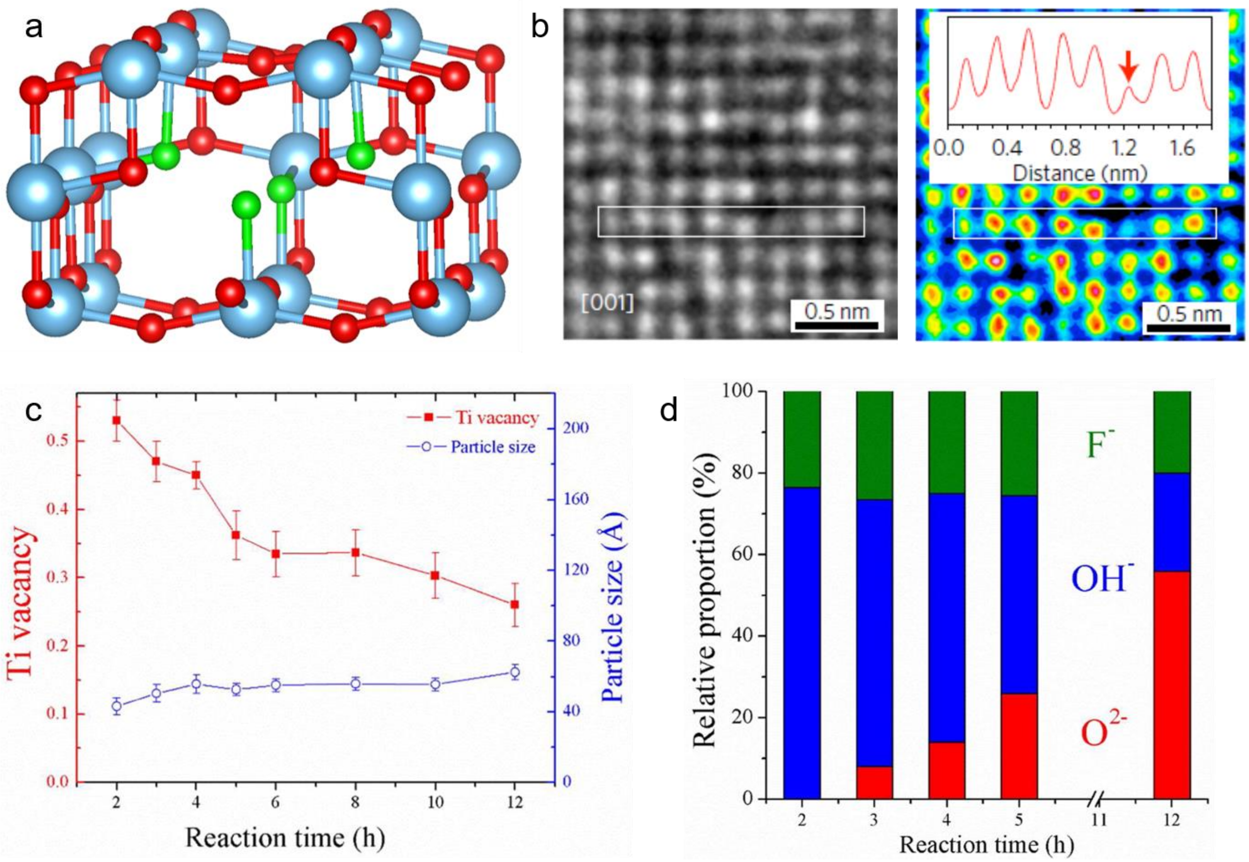

Figure 2. a) Structural representation of the anatase structure featuring a vacancy stabilized by the substitution of four oxide- (red spheres) by four fluoride ions (green spheres). b) High-resolution TEM image and a colored version showing the variation in the Ti atomic occupancy. Reprinted with permission from ref [3]. Copyright 2017 Nature Publishing Group. c) Evolution of the titanium vacancy content and particle size of the anatase phase upon reaction. Adapted from ref [2]. Copyright 2016 American Chemical Society. d) Evolution of the relative proportions of anions in the anatase phase upon reaction. Adapted from ref [2]. Copyright 2016 American Chemical Society.

To extend this study to chemical processes typically encountered in the literature for the synthesis of anatase crystals with tailored facets, we investigated the effect of the temperature.[22] Upon increasing the temperature from 90 °C (typically used for our reference compound, see later) to

190 °C, we observed a decrease of the content of cationic vacancies through dehydroxyfluorination processes according to:

$$Ti_{1-x-y}\square_{x+y}O_{2-4(x+y)}F_{4x}(OH)_{4y} \rightarrow (1-x-y)\cdot TiO_2 + 4x\cdot HF + 2(y-x)\cdot H_2O$$

The above reaction, however, was shown to be incomplete even at 190 °C with fluoride remaining in the framework (up to 4 wt.%). Therefore, we concluded that given synthesis conditions typically utilized in the literature, the stabilization of an oxyfluoride phase composition is very likely. Note that an increase of the synthesis temperature was accompanied with not only a change of the chemical composition but also the morphology.[22]

Overall, we have demonstrated that solvothermal conditions employing fluoride-based precursors can lead to a phase composition that deviates from the ideal "TiO_2", with a particular emphasis on the stabilization of vacancies by an anionic-driven charge-compensating mechanism.

2.2. Structural features

Having established the stabilization of cationic vacancies as well as fluoride and hydroxide ions within the anionic sublattice, we detail the atomic local arrangement of these species, focusing on our prototype phase composition $Ti_{0.78}\square_{0.22}O_{1.12}F_{0.40}(OH)_{0.48}$. Owing to the properties of the ^{19}F nucleus (100% natural abundance, high gyromagnetic ratio, and chemical shift range spanning 800 ppm), solid-state ^{19}F NMR was used to assess local atomic-scale structure in the material. The typical ^{19}F NMR spectrum **(Figure 3a)** shows three lines with different isotropic chemical shift (δ_{iso}) values. These lines were attributed to a varying content of Ti and vacancies surrounding fluoride ions, with Ti_3-F (- 88 ppm), $Ti_2\square_1$-F (-4 ppm) and $Ti_1\square_2$-F (98 ppm) species, providing evidences for the stabilization of single and paired-vacancies (see inset **Figure 3a**).[1] These assignments were made according to the probabilities of occurrence of the various anionic coordination environments and the expected decrease of the chemical shift of the anion when the number of surrounding cations increases as demonstrate with reference compounds.[1]

From the integrated line intensities, we observed a preferential ordering of fluoride ions close to vacancies, minimizing electrostatic repulsions between anions oriented toward the vacancy as compared to O^{2-} ions. This fluoride-vacancy ordering was further confirmed by DFT-calculations.[1,23] In specific, static DFT calculations were performed on a $Ti_{127}\square_1F_4O_{252}$ supercell, in which the relative energies of five different O/F arrangements were compared **(Figure 3b)**. The energy reference was chosen for the configuration where the vacancy is surrounded by six O^{2-} ions. The effect of the local anionic environment on the energy was then monitored by progressively substituting O^{2-} by F^-, pointing to a continuous stabilization of the vacancy by F atoms, in good agreement with solid-state ^{19}F NMR. In addition, DFT-calculations captured structural features such as Ti-F bond lengths.[1,23,3] As expected, Ti-F distances increase with the number of neighboring Ti^{4+} ions from 1.81 Å for $Ti_1\square_2$-F, 2.00 Å for $Ti_2\square_1$-F to 2.12 Å for three-fold Ti_3-F species. This point highlights a variation of the iono-covalent character of Ti-F bonds. Concerning OH groups, we identified Ti_3-OH, $Ti_2\square_1$-OH and $Ti_1\square_2$-OH species by ^1H NMR.[22] The relative intensities pointed to the dominance of $Ti_2\square_1$-OH and Ti_3-OH species, which is in good agreement with ^{19}F NMR, *i.e.*, the dominance of $Ti_2\square_1$-F and $Ti_1\square_2$-F species.

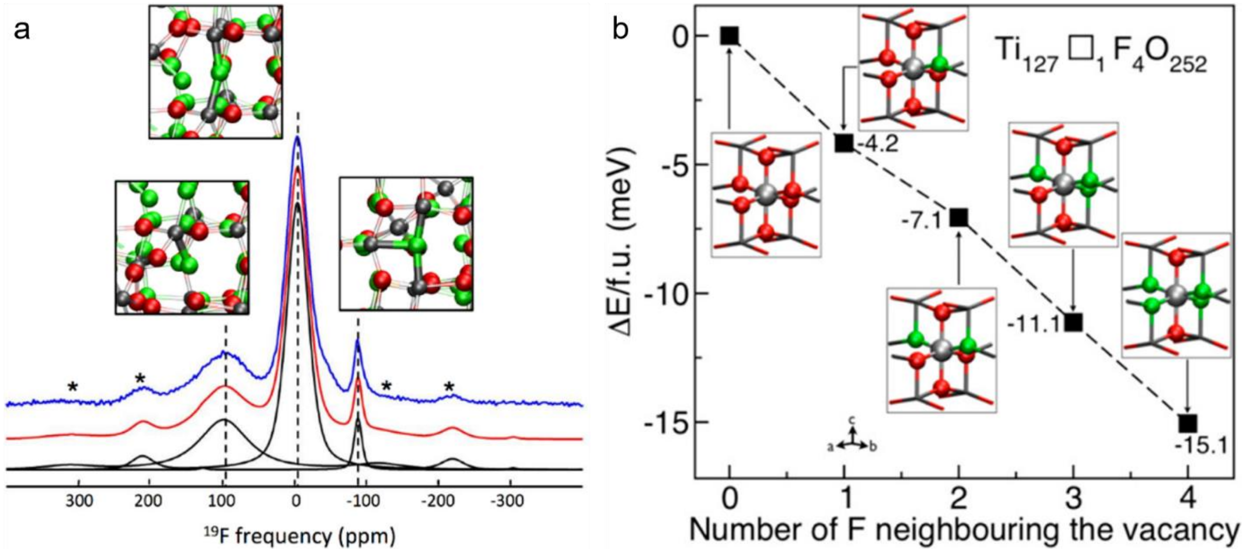

Figure 3. a) Experimental (in blue) ^{19}F solid state MAS NMR spectrum of anatase $Ti_{0.78}\square_{0.22}O_{1.12}F_{0.40}(OH)_{0.48}$, fitted (in red) with three NMR lines (in black, indicated by vertical dashed lines), which are assigned to $Ti_1\square_2$-F, $Ti_2\square_1$-F and Ti_3-F (from left to right). The asterisks indicate the spinning sidebands. Corresponding structures extracted from a DFT-based molecular dynamics simulation are also shown (grey: Ti, green: F and red: O, on each snapshot the illustrated bonds are shown as thick solid cylinders, while the other bonds are shown as thin transparent cylinders. b) DFT calculations performed on a $Ti_{127}\square_1F_4O_{252}$ supercell containing one vacancy □ (light gray) was built by replacing four O atoms (red) with four F atoms (green). The anionic environment was tuned by adding F in the vicinity of the vacancy. In all cases, the F atoms that were not placed around the vacancy substituted for random O atoms in the lattice and, thus, had the Ti_3-F environment. The sticks in the snapshots link the central vacancies to their neighboring atoms (only the six atoms around the vacancy are drawn). Adapted from ref [1]. Copyright 2015 American Chemical Society.

3. ION-INTERCALATION PROPERTIES

3.1. Modifying the lithium insertion mechanism

The electrochemical insertion of lithium ions within the anatase framework has been widely investigated. It occurs via a phase transition from tetragonal to the orthorhombic (space group: *Imma*) Li-rich titanate $Li_{0.5\pm\alpha}TiO_2$, characterized by a potential - composition plateau.[24,25] Reducing the crystal size has been demonstrated to change the lithium storage mechanism from the phase-transition to a solid-solution behavior characterized by a continuous change of the potential-composition curve.[26,27] Interestingly, the compound $Ti_{0.78}\square_{0.22}O_{1.12}F_{0.40}(OH)_{0.48}$ features particle sizes of 6-9 nm that typically would undergo a phase transition[26] providing a case study to investigate the effect of cationic vacancies on the lithium storage mechanism. The later was investigated by means of galvanostatic intermittent titration technique (GITT) and structural analysis of a discharged electrode. The quasi-equilibrium voltage obtained by GITT **(Figure 4a)** showed a smooth curve, in contrast to the plateau characterizing a phase transition, indicating that lithium ions are inserted via a continuous solid-solution behavior. This mechanism was further supported by the PDF analysis of the discharged electrode confirming the absence of the orthorhombic structure **(Figure 4b)**.

To understand the observed solid solution Li storage mechanism, one can recall that as shown by Morgan et *al*[28], the phase transition occurring during the lithium insertion in defect-free anatase arises from a pairing effect of edge-sharing LiO_6 octahedra occupying interstitial sites. Accordingly, two main factors contributing to the observed change of storage mechanism could be identified: the presence of cationic vacancies that act as additional host sites and the occurrence of heteroanionic environments at both the interstitial and vacancies host sites. First, the intercalation of Li^+ ions within titanium vacancy sites was demonstrated by ^{19}F NMR, *i.e.*, through the disappearance of the lines characterizing the presence of vacancies in the vicinity of fluoride ions. Secondly, low scan cyclic voltammetry performed on cation-deficient anatase revealed broader and new redox peaks as compare to the defect-free anatase **(Figure 4c)**. Using DFT-calculations, this variation of lithium insertion energies has been explained by the changes of the local anionic environments around Li^+ ions, with notably an increase of the redox potential in fluoride-rich intercalation site (see section 3.4.).[29]

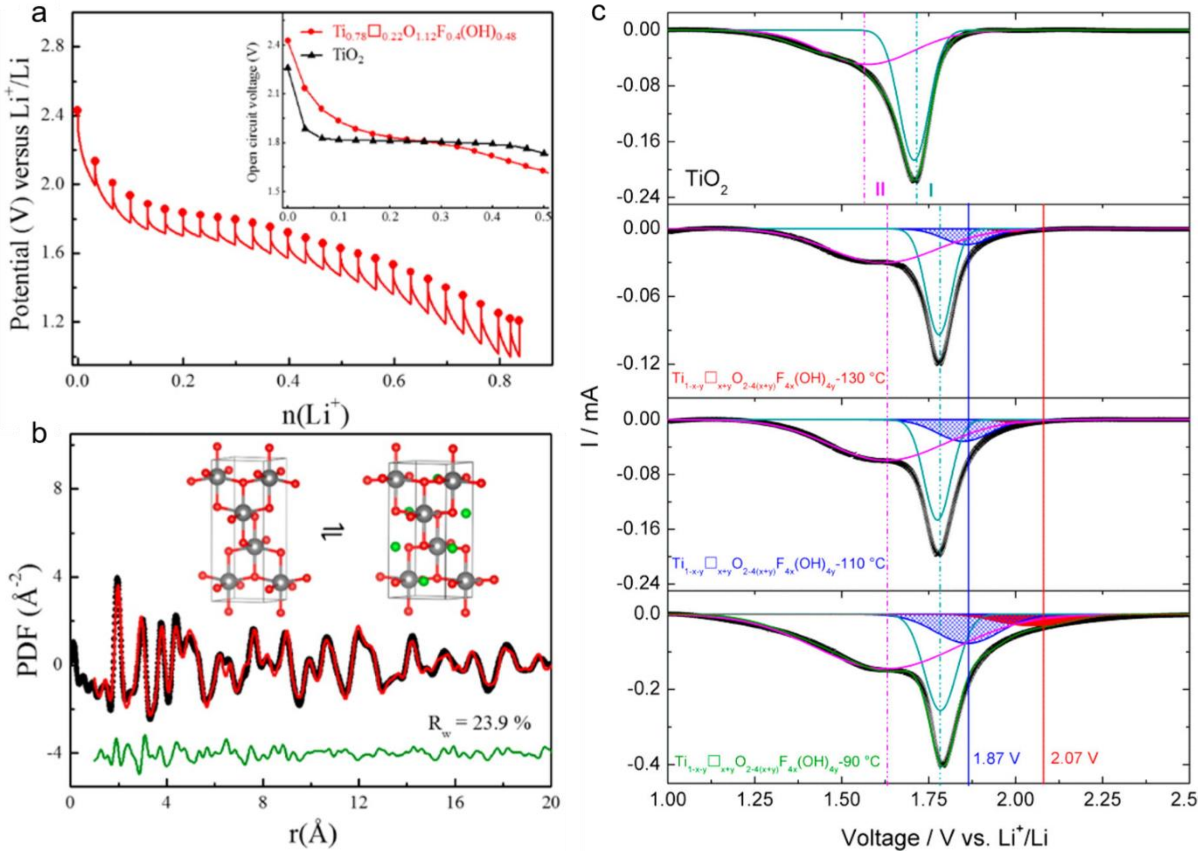

Figure 4. a) Quasi-equilibrium voltage obtained by GITT for $Ti_{0.78}\square_{0.22}O_{1.12}F_{0.40}(OH)_{0.48}$ and TiO_2 (see inset). b) Real-space refinement of the PDF data obtained for a discharged electrode. Adapted from ref [1]. Copyright 2015 American Chemical Society. c) Slow scanning liner sweep voltammetries (0.05 mV s^{-1}) of defect-free TiO_2 and $Ti_{1-x-y}\square_{x+y}O_{2-4(x+y)}F_{4x}(OH)_{4y}$ anatase prepared at different temperatures (130, 110, and 90 °C, with an increasing content of cationic vacancies).

The sample prepared at 90 °C refers to $Ti_{0.78}\square_{0.22}O_{1.12}F_{0.40}(OH)_{0.48}$. Adapted from ref [29]. Copyright 2018 American Chemical Society.

3.2. Unlocking the electrochemical intercalation of Mg^{2+} and Al^{3+}-ions

The development of post lithium-ion insertion chemistries implies the use of other charge carriers such as Mg^{2+} and Al^{3+} polyvalent ions.[30] The expected beneficial uses of these charge carriers include a greater abundance than lithium and a higher volumetric energy density owing to the use of the corresponding metal at the negative electrode with multi-electron transfers. The major hurdle to the utilization of polyvalent ions, however, is due to the poor solid-state diffusion of these ions within atomic structures. This can be explained by increasing electrostatic interaction between these cations and the anionic sublattice. To tackle this issue, we proposed the use of cation-deficient materials as a way to promote the insertion and solid-state diffusion of Mg^{2+} and Al^{3+}-ions.[3] Cationic vacancies provide additional insertion host sites and an increasing diffusion pathway. From a thermodynamic perspective, we have demonstrated by DFT-calculations favorable intercalation energies in vacancies for Mg^{2+} and Al^{3+} as compare to native interstitial sites **(Figure 5a)**. Note that we have observed a similar trend with Na^{+} ions.[31] Using galvanostatic experiments with a three-cell configuration and non-aqueous electrolytes, we established that cation-deficient anatase can intercalate Mg^{2+} and Al^{3+} with a significant improvement of the capacity, *i.e.*, number of intercalated ions **(Figure 5b,c)**.

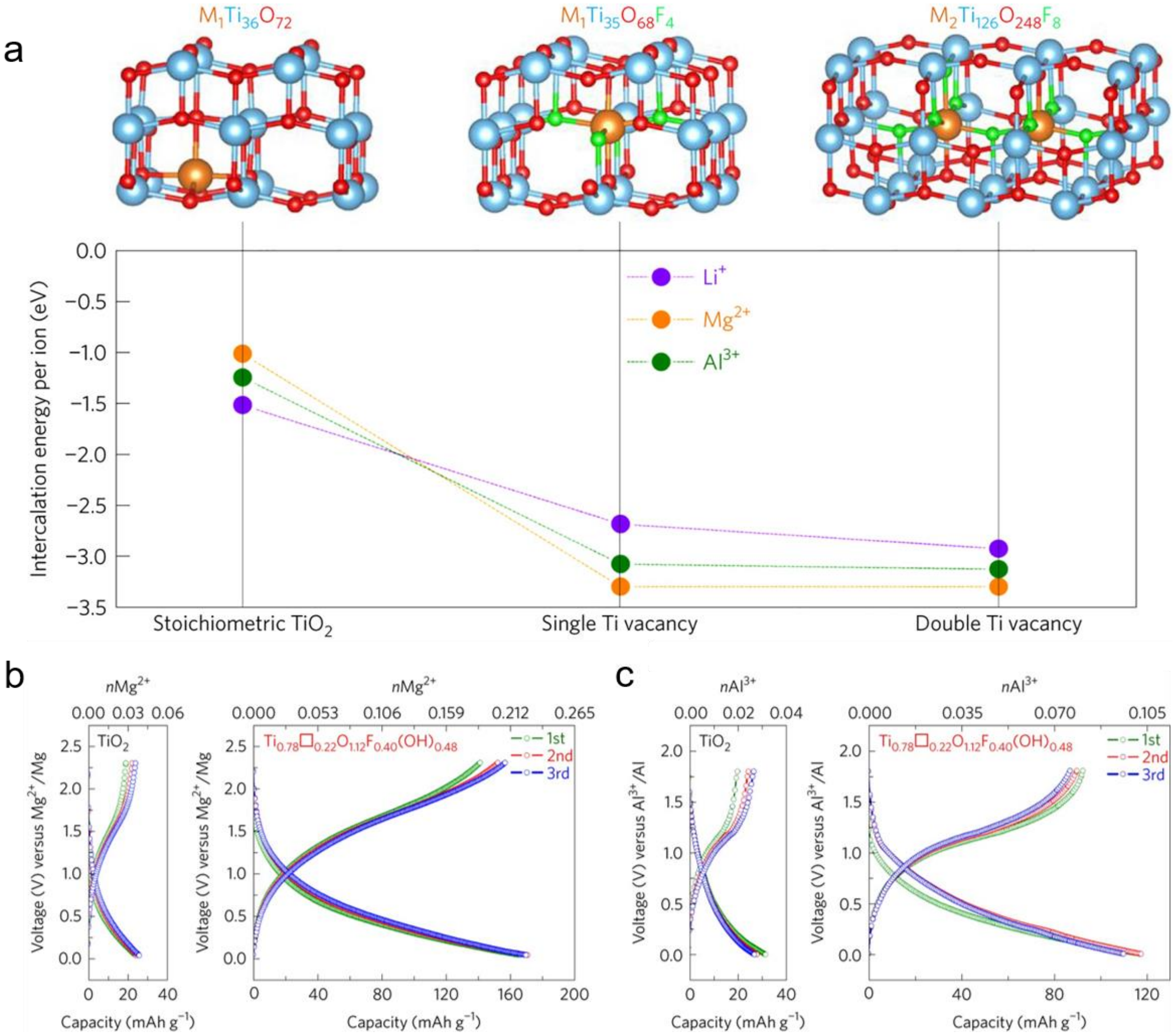

Figure 5. a) Bottom: DFT-calculated intercalation energies for Li^+, Mg^{2+}, Al^{3+} in anatase and in cation-deficient TiO_2. Top: from left to right, corresponding structural representations of the intercalation sites in TiO_2 (defect-free), single-vacancy $Ti_{35}\square_1O_{68}F_4$ and double-vacancy $Ti_{126}\square_2O_{248}F_8$ anatase. Galvanostatic discharge-charge curves for TiO_2 and $Ti_{0.78}\square_{0.22}O_{1.12}F_{0.40}(OH)_{0.48}$ in b) Mg- and c) Al-cells. Reprinted with permission from ref [3]. Copyright 2017 Nature Publishing Group.

The investigation of Mg^{2+} and Al^{3+} ion-intercalation mechanisms highlighted qualitive different behaviors[3,4] that will be detailed below. Concerning Mg^{2+}-ions, the location of ions during the course of the discharge reaction was monitored by means of *ex situ* structural analysis. The PDF data were refined considering the location of Mg^{2+} within the titanium site (4a Wyckoff site), *i.e.*, within the titanium vacancies, and within the native interstitial site (4b Wyckoff site). The results **(Figure 6a)** demonstrated that Mg^{2+} ions are preferentially inserted within the titanium vacancies, filling the corresponding 4b site at the expense of the 4a site, in good agreement with DFT-calculations. While Mg^{2+} can fully occupy all available titanium vacancies, the number of Al^{3+}-inserted suggested a different ion storage mechanism with barely half of the number of Al^{3+} ions inserted as compare to Mg^{2+}, *i.e.*, ~ 0.1 Al^{3+} and ~0.23 Mg^{2+}. The first evidence of an unique storage mechanism displayed by Al^{3+} ions was observed by structural analysis of a discharged electrode by means of PDF refinement **(Figure 6b)**. In the latter, we noticed that the local structure featured inter-atomic distances that could not be captured by those of an anatase framework. Particularly noteworthy were distances located at ~ 1.83 and 2.6 Å, which were assigned to Al-X and anion-anion distances, respectively. The refinement of Al^{3+} occupancy yielded 0.11(3) at the titanium 4a and 0.02(2) at the 4b interstitial sites. Considering the uncertainty of these data, we utilized ^{27}Al and ^{19}F NMR **(Figure 6c)** to better understand the Al^{3+} insertion storage mechanism. Remarkably, Al^{3+}-insertion induced the disappearance of the ^{19}F NMR line assigned to $Ti_1\square_2$-F. The line assigned to $Ti_2\square_1$-F, however, remained almost unchanged leading to the conclusion that Al^{3+} ions could not fill both vacancies. Using DFT-calculations, we showed an enhanced thermodynamic driving force for the insertion of one Al^{3+} ion into of the two paired-vacancies. The insertion of this ion, however, produced a strong contraction of the anion positions around it, matching the distances observed by PDF, and in turn, expanding the available site volume of the adjacent paired vacancy **(Figure 6d)**. The insertion of a second Al^{3+} ion was shown to be less favorable yielding unfavorable F coordination mode and ruling out the full occupancy of the paired vacancy. This work put into perspectives the specific structural features induced by the intercalation of highly polarizing Al^{3+} ions.[4]

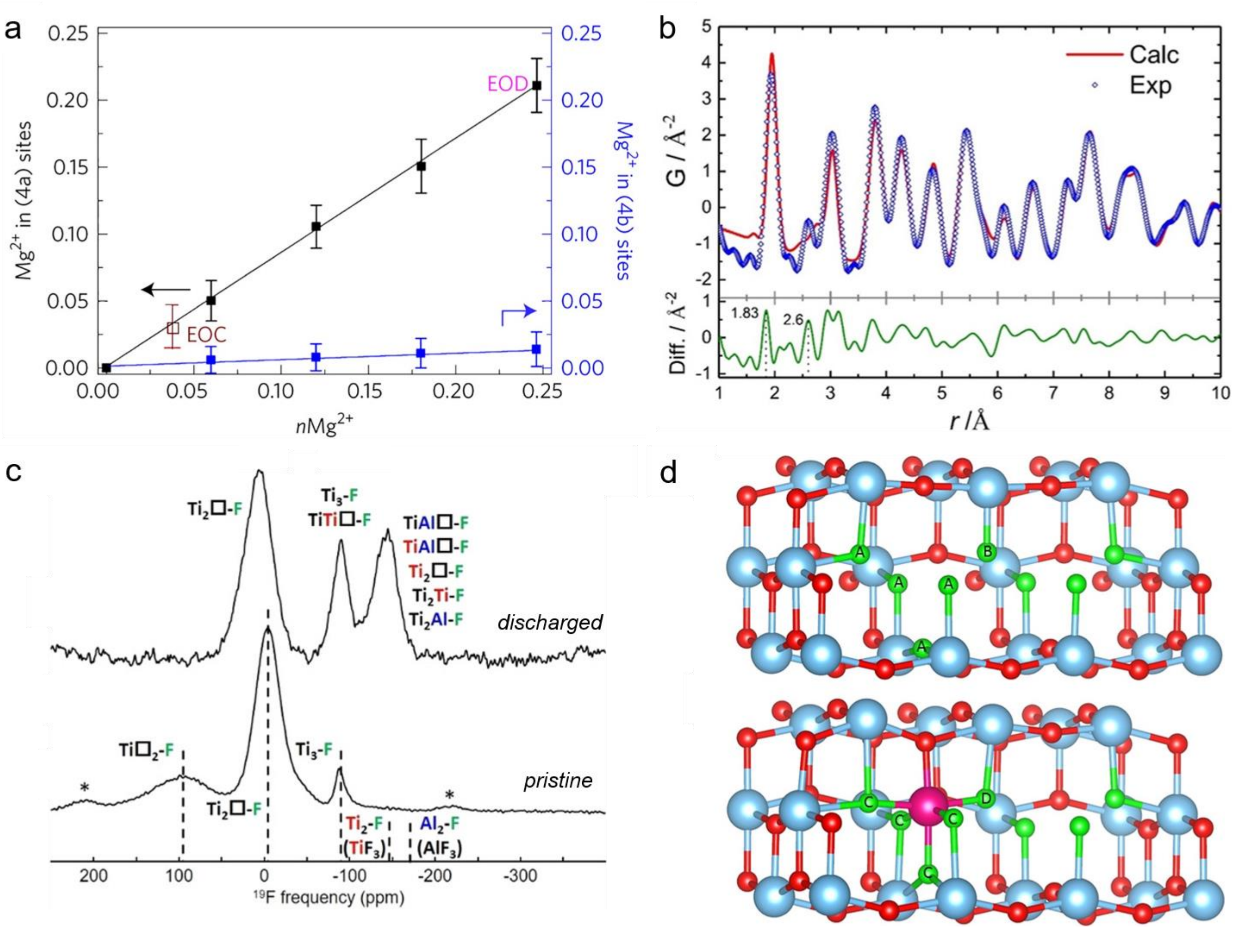

Figure 6. a) Mg^{2+} ion occupancy within the titanium (4a) and interstitial (4b) sites obtained by PDF refinements of discharged/charged electrodes. Reprinted with permission from ref [3]. Copyright 2017 Nature Publishing Group. b) PDF refinement performed on an Al^{3+}-inserted electrode. c) ^{19}F NMR spectra of pristine (bottom) and discharged electrode. d) Structural representations of the supercell featuring double vacancy $Ti_{126}\square_2O_{248}F_8$ before (a) and after (b) the introduction of one Al^{3+}, *i.e.*, $Ti_{126}\square_1Al_1O_{248}F_8$. The blue, red, green and magenta spheres represent titanium, oxygen, fluorine and aluminum atoms, respectively. Labels A–D refer to (A)

bridging F-species $Ti_2\square$-F, (B) terminal F in $Ti\square_2$-F, (C) F-species in Ti_2Al-F and (D) F-species in $TiAl\square$-F. (b,c,d) Reprinted with permission from ref [4]. Copyright 2020 John Wiley and Sons.

3.3. Competitive intercalation in dual Mg-Li ions batteries

Having established a thermodynamical driving force for ion-insertion at vacancy sites, we posed the question about dual Li^+-Mg^{2+} ions storage mechanism.[32] To answer this question, we investigated the electrochemical properties of $Ti_{0.78}\square_{0.22}O_{1.12}F_{0.40}(OH)_{0.48}$ compound in a dual-ion battery, *e.g.*, an electrochemical cell comprising an Mg-anode, a cation-deficient anatase material as the positive electrode and a hybrid dual-ion electrolyte consisting of an all-phenyl complex (APC) $Mg_2Cl_3^+AlPh_2Cl_2^-$ in tetrahydrofuran (THF) with LiCl as the Li source. The measured capacity obtained by galvanostatic experiments was found to depend of the Li^+ concentration, reaching the full utilization of the Ti^{4+}/Ti^{3+} redox couple (~ 290 mAh g^{-1}) at 1 M LiCl. The investigation of the dual-ion storage mechanism (for 0.2 M LiCl) highlighted a co-insertion of Mg^{2+} and Li^+ ions during the discharge process **(Figure 7)**. As opposed to Mg-cell, where Mg^{2+} ion fully occupied Ti vacancy[3], we noticed a small content of Li^+ within the vacancy site, *i.e.*, 0.04 Li^+ and 0.18 Mg^{2+}. DFT-calculations predicted a dual-ion insertion mechanism in paired vacancies for a certain range of lithium and magnesium electrochemical potentials. It further showed that for a staged insertion, the filling of the second vacancy site is less favorable than the first one. Such effect was rationalized based on local structural distortion induced by the first cation insertion, which then makes the second insertion less favorable. Before cation insertion, the vacant sites are tetragonally distorted. The insertion of the first cation induces a reduction of this distortion along with an increased distortion of the neighboring still-vacant site. This effect has been shown to be stronger for Mg^{2+}. This study further demonstrated that the implementation of cationic vacancies is an effective approach to increase the energy density of dual-ion batteries.

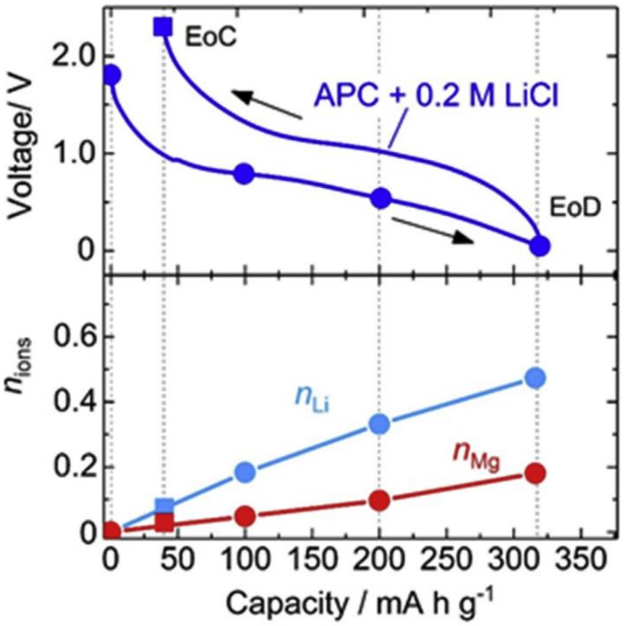

Figure 7. Galvanostatic discharge-charge curves and chemical analyses (ICP-AES) of Li, Mg contents during the first cycle. The electrolyte was APC with 0.2M of LiCl. Reprinted with permission from ref [32]. Copyright 2020 Elsevier.

3.4. Critical role of host sites (vacancies/interstitials) local anionic environments

The charge-compensating mechanism in $Ti_{0.78}\square_{0.22}O_{1.12}F_{0.40}(OH)_{0.48}$ enabled the stabilization of vacancies that, as shown above, can act as host sites for ion intercalation. In addition, the anionic sublattice with vacancies results in complex structural features associated with new types of anion coordination modes and a preferential location of monovalent ions to be close to the vacancy sites. Considering the chemical composition $Ti_{0.78}\square_{0.22}O_{1.12}F_{0.40}(OH)_{0.48}$, it is expected that different anionic environments exist within the vicinity of vacancies and interstitial sites. To illustrate this point, we assumed a simple random distribution of the anions around the vacancy **(Figure 8a)** showing that a heterogeneous anionic distribution is expected to occur. Such a distribution was shown to affect the intercalation energies of ions as illustrated in the case of Li^+ **(Figure 8b)** and Al^{3+} **(Figure 8d)**.[29,4] More specifically, **Figure 8b** shows the intercalation energies obtained by

DFT-calculations for Li^+ ions sitting in cationic vacancies having different anionic environments (supercell $Ti_{35}\square_1O_{68}X_4$ with the Ti vacancy coordinated by 2O and X=4F, 1OH + 3F, 2OH + 2F, 3OH + 1F, 4OH). Remarkably, the intercalation energy is strongly dependent on the anionic environment surrounding the vacancy, with a more favorable energy for fluoride-rich environment that tends to decrease upon hydroxylation. In the case of Al^{3+} ions, we observed the same trend **(Figure 8d)**. Moreover, the anionic environment influences the position of the ion within the octahedral site as shown, for example, for Mg^{2+} ions sitting in hydroxylated and fluorinated vacancy sites **(Figure 8c)**, and in turn the redox potentials.[33] Such an effect was also observed for an interstitial site adjacent to a vacancy **(Figure 8c)**: the presence of monovalent ion affects the redox potential of the interstitial site. This trend was also observed for Al^{3+} ions and whatever the anionic environment of the neighbored vacancy. As shown in **Figure 8d,** the grey points represent intercalation energies at interstitial sites adjacent to vacancies having different anionic environments and the horizontal dashed line show the intercalation energy for Al^{3+} in defect-free anatase.[4] The comparison confirms the significant impact of the anionic environment on the intercalation energy.

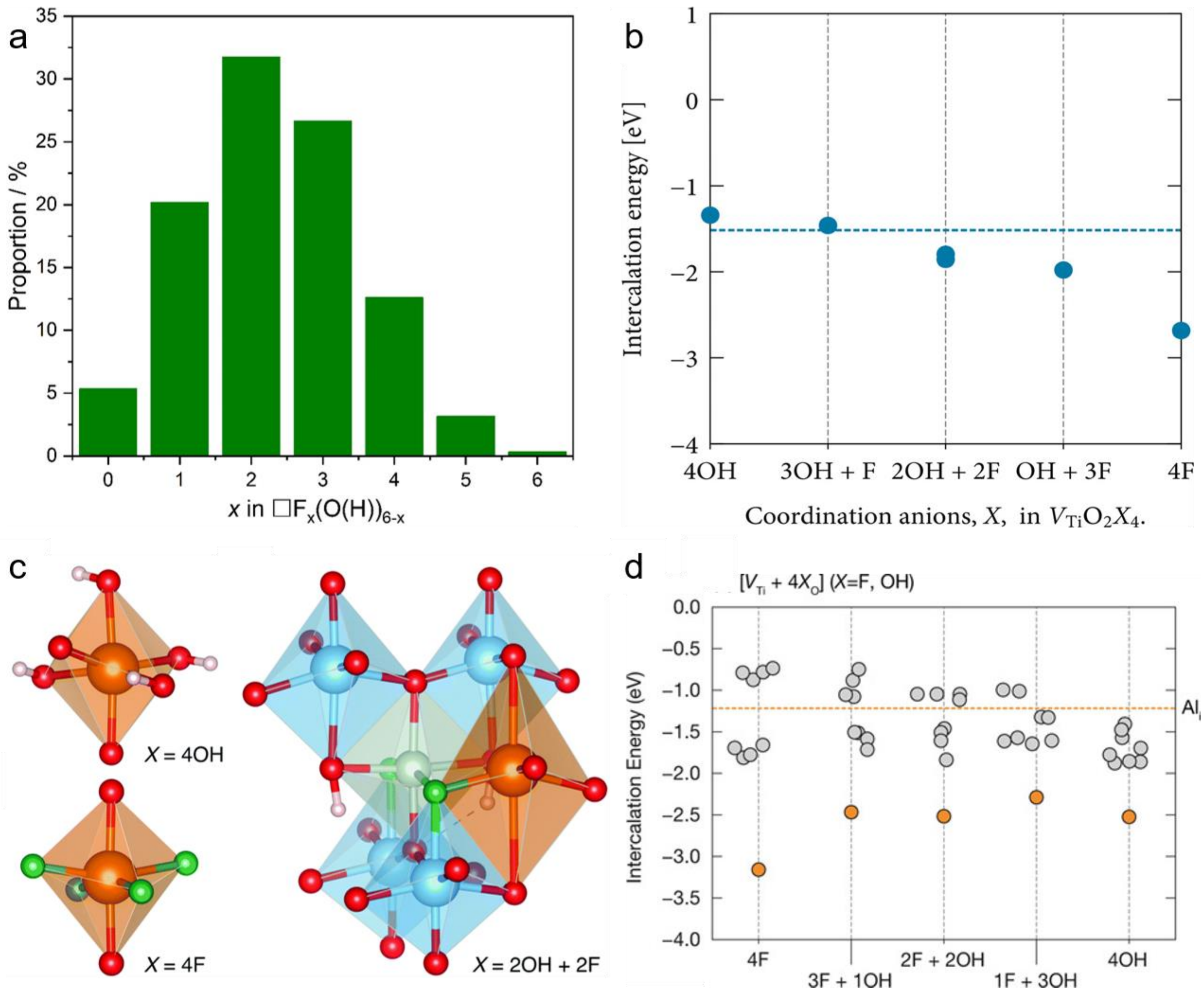

Figure 8. a) Vacancy anionic environments assuming a random distribution. Adapted from reference [33]. Copyright 2018 Royal Society of Chemistry. b) Ion intercalation energies of Li^+ in a vacancy site featuring different anionic environments. The horizontal dashed line represents the intercalation energy in stoichiometric TiO_2. Reprinted with permission from ref [29]. Copyright 2018 American Chemical Society. c) Optimized structures of Mg^{2+} occupying vacancy sites surrounded by 4F, 4OH and Mg^{2+} occupying an interstitial site close to a cationic vacancy (grey). Reprinted with permission from ref [33]. Copyright 2018 Royal Society of Chemistry. d) Al^{3+} intercalation energies in a vacancy site featuring different anionic environments. The horizontal dashed line represents the intercalation energy in stoichiometric TiO_2. The grey points represent intercalation

energies at interstitial sites adjacent to a vacancy. Reprinted with permission from ref[4]. Copyright 2020 John Wiley and Sons.

4. PERSPECTIVES

This Account first focused on the relationships between the synthesis and structure of the anatase framework highlighting a charge-compensating mechanism enabling the stabilization of high and controllable content of cationic vacancies. The accurate determination of the phase composition through multiple analytical and physical characterizations allowed to a better understanding of the impact of the synthesis parameters (temperature, fluoride precursors, duration time) on the unique structural features of cation-deficient anatase. The underlying connection between the synthesis and the phase composition is extendable to other types of materials as a primary step to finely describe the structural features and hence rationalize properties.

To extend the family of cation-deficient materials, two main synthetic approaches can be considered: through low-valent anionic substitution and high-valent cationic inclusion. Although, it is know that certain types of crystal lattices, such as the spinel structure, are naturally prone to accommodate cationic vacancies, further studies may be based on the identification of frameworks capable of hosting a large content of vacancies, a wide range of elements, oxidation states and in turn various phase compositions, *i.e.*, adaptable frameworks[34]. Moreover, the understanding of the formation mechanism of highly defective compounds could be considered as well to better understand how cationic vacancies are involved in the growth of inorganic nanoparticles.[35,36]

The use of cationic vacancies has emerged as an effective strategy to improve the electrochemical properties of electrode materials as reviewed by Hahn et *al*[11] and Gao et *al*[37]. As shown in these reviews, defect engineering has been demonstrated for different charge carriers spanning proton, monovalent and polyvalent ions. Rationalizing the observed enhanced/modified properties implies that cationic-deficient materials are well described. It would certainly lead to a better understanding of fundamental aspects such as diffusion[38] phenomena and more efficient electrochemical systems. Last but not least, it would be pertinent to investigate the long-term and cycle stability of cation vacancies to further promotes their use in energy storage devices.

The characterization of cationic vacancies implies different structural features occurring at various length scales **(Figure 9)**. A vast array of experimental techniques can be used to characterize cationic vacancies. In the following, some of these techniques are illustrated. In addition to the phase composition, the presence of these vacancies can be deduced from the refinement of the atomic structure of X-ray/neutron diffraction data provided that their concentration is sufficiently high to be detected. X-ray/neutron PDF can be used to quantify their presence[29] and capture local distortion as shown for example in the case of MnO_2[39]. Similarly, extended X-ray absorption fine structure can be used to demonstrate their presence and the local distortion associated.[40,41] The formation of cluster of vacancies, *i.e.*, di- and tri-vacancies, can be revealed by high resolution transmission electron microscopy as shown for MnO_2[42] and more recently, for monolayer $Ti_3C_2T_x$ flakes[43]. Through variation of the isotropic chemical shift values, NMR can be used to discern the presence of cationic vacancies as shown here in the case of cation-deficient anatase[1] or in the case of Prussian blue analogues[44]. Overall, although techniques are available to appreciate the presence, concentration and clustering of vacancies, a description of their local environment is more challenging. Of interest is the description of anionic environments including cation-anion distribution and bond distances around the vacancy along with its volume. Such quantities are hardly appreciable using experimental techniques and require the use of computational models[1,3,23,43]. Building structural models that approach the complexity of experimental compounds is, however, particularly challenging due to a large set of atomic structure combinations[23] and nonetheless, modern computational tools could certainly play an important role in understanding cationic-deficient materials. Finally, at the mesoscopic scale, it is anticipated that vacancies form extended microporous networks. Understanding the nature of long-range vacancy correlations[45] will be an even more challenging aspect to capture percolation pathways implied in mass transport and storage properties.

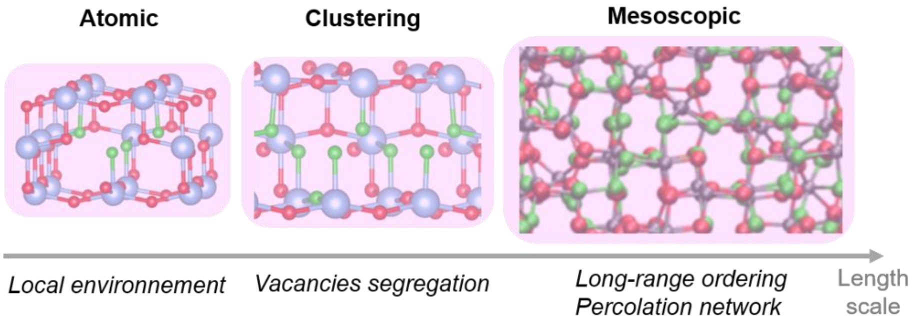

Figure 9. Structural features of cationic vacancies with respect to various length scales.

AUTHOR INFORMATION

Corresponding Author

* damien.dambournet@sorbonne-universite.fr

Funding Sources

These works were supported by European Union's Seventh Framework Programme (FP7/2007-2013) under REA Grant Agreement No. 321879 (FLUOSYNES) and the French National Research Agency under Idex@Sorbonne University for the Future Investments program (No. ANR-11- IDEX-0004-02).

Notes

The author declares no competing financial interest.

Biography

Damien Dambournet is an associate professor in the PHENIX laboratory at Sorbonne Université. He received his Ph.D. diploma (physical-chemistry of condensed matter) from the Institute of Condensed Matter of Bordeaux (ICMCB) under the supervision of A. Tressaud and A. Demourgues in 2008. After graduation, he was a postdoctoral appointee at Argonne National Laboratory supervised by K. Amine and I. Belharouak. Since 2011, his research covers several topics in the field of inorganic solid-state chemistry, including the synthesis of disordered materials featuring defects, heteroanionic composition, with an emphasize on the relationships between synthesis, structure and electrochemical properties.

ACKNOWLEDGMENT

The author wishes to thank the French network on fluorine chemistry (GIS-fluor) and the RS2E for continuous support. The works presented herein have implied numerous collaborators that are thank for their valuable contribution: Wei Li, Jiwei Ma, Dario Corradini, Mathieu Salanne, Alain Demourgues, Toshirari Kokestu, Peter. Strasser, Olaf J. Borkiewicz, Monique Body, Christophe Legein, Ben. J. Morgan. Special thanks to C. Legein for his remarkable contribution and our many discussions.

REFERENCES

(1) Li, W.; Corradini, D.; Body, M.; Legein, C.; Salanne, M.; Ma, J.; Chapman, K. W.; Chupas, P. J.; Rollet, A.-L.; Julien, C.; Zhagib, K.; Duttine, M.; Demourgues, A.; Groult, H.; Dambournet, D. High Substitution Rate in TiO_2 Anatase Nanoparticles with Cationic Vacancies for Fast Lithium Storage. *Chem. Mater.* **2015**, *27*, 5014–5019.

(2) Li, W.; Body, M.; Legein, C.; Borkiewicz, O. J.; Dambournet, D. Atomic Insights into Nanoparticle Formation of Hydroxyfluorinated Anatase Featuring Titanium Vacancies. *Inorg. Chem.* **2016**, *55*, 7182–7187.

(3) Koketsu, T.; Ma, J.; Morgan, B. J.; Body, M.; Legein, C.; Dachraoui, W.; Giannini, M.; Demortière, A.; Salanne, M.; Dardoize, F.; Groult, H.; Borkiewicz, O. J.; Chapman, K. W.; Strasser, P.; Dambournet, D. Reversible Magnesium and Aluminium Ions Insertion in Cation-Deficient Anatase TiO_2. *Nat. Mater.* **2017**, *16*, 1142.

(4) Legein, C.; Morgan, B. J.; Fayon, F.; Koketsu, T.; Ma, J.; Body, M.; Sarou-Kanian, V.; Wei, X.-K.; Heggen, M.; Borkiewicz, O. J.; Strasser, P.; Dambournet, D. Atomic Insights into Aluminium-Ion Insertion in Defective Anatase for Batteries. *Angew. Chem. Int. Ed.* **2020**, *59*, 19247–19253.

(5) Bruce, P. G. Solid-State Chemistry of Lithium Power Sources. *Chem. Commun.* **1997**, No. 19, 1817–1824.

(6) Whittingham, M. S. Electrical Energy Storage and Intercalation Chemistry. *Science* **1976**, *192*, 1126–1127.

(7) Mizushima, K.; Jones, P. C.; Wiseman, P. J.; Goodenough, J. B. Li_xCoO_2 ($0<x<1$): A new cathode material for batteries of high energy density. *Mater. Res. Bull.* **1980**, *15*, 783–789.

(8) Li, B.; Sougrati, M. T.; Rousse, G.; Morozov, A. V.; Dedryvère, R.; Iadecola, A.; Senyshyn, A.; Zhang, L.; Abakumov, A. M.; Doublet, M.-L.; Tarascon, J.-M. Correlating Ligand-to-Metal Charge Transfer with Voltage Hysteresis in a Li-Rich Rock-Salt Compound Exhibiting Anionic Redox. *Nat. Chem.* **2021**, *13*, 1070–1080.

(9) Mortemard de Boisse, B.; Reynaud, M.; Ma, J.; Kikkawa, J.; Nishimura, S.; Casas-Cabanas, M.; Delmas, C.; Okubo, M.; Yamada, A. Coulombic Self-Ordering upon Charging a Large-Capacity Layered Cathode Material for Rechargeable Batteries. *Nat. Commun.* **2019**, *10*,

(10) House, R. A.; Maitra, U.; Pérez-Osorio, M. A.; Lozano, J. G.; Jin, L.; Somerville, J. W.; Duda, L. C.; Nag, A.; Walters, A.; Zhou, K.-J.; Roberts, M. R.; Bruce, P. G. Superstructure Control of First-Cycle Voltage Hysteresis in Oxygen-Redox Cathodes. *Nature* **2020**, *577*, 502–508.

(11) Hahn, B. P.; Long, J. W.; Rolison, D. R. Something from Nothing: Enhancing Electrochemical Charge Storage with Cation Vacancies. *Acc. Chem. Res.* **2013**, *46*, 1181–1191.

(12) Wagemaker, M.; Kentgens, A. P. M.; Mulder, F. M. Equilibrium Lithium Transport between Nanocrystalline Phases in Intercalated TiO_2 Anatase. *Nature* **2002**, *418*, 397–399.

(13) Wu, L.; Buchholz, D.; Bresser, D.; Gomes Chagas, L.; Passerini, S. Anatase TiO_2 Nanoparticles for High Power Sodium-Ion Anodes. *J. Power Sources* **2014**, *251*, 379–385.

(14) Li, W.; Fukunishi, M.; Morgan, Benjamin. J.; Borkiewicz, O. J.; Chapman, K. W.; Pralong, V.; Maignan, A.; Lebedev, O. I.; Ma, J.; Groult, H.; Komaba, S.; Dambournet, D. A Reversible Phase Transition for Sodium Insertion in Anatase TiO_2. *Chem. Mater.* **2017**, *29*, 1836–1844.

(15) Yang, H. G.; Sun, C. H.; Qiao, S. Z.; Zou, J.; Liu, G.; Smith, S. C.; Cheng, H. M.; Lu, G. Q. Anatase TiO_2 Single Crystals with a Large Percentage of Reactive Facets. *Nature* **2008**, *453*, 638–641.

(16) Liu, G.; Yang, H. G.; Pan, J.; Yang, Y. Q.; Lu, G. Q. (Max); Cheng, H.-M. Titanium Dioxide Crystals with Tailored Facets. *Chem. Rev.* **2014**, *114*, 9559–9612.

(17) Ong, W.-J.; Tan, L.-L.; Chai, S.-P.; Yong, S.-T.; Mohamed, A. R. Highly Reactive {001} Facets of TiO_2-Based Composites: Synthesis, Formation Mechanism and Characterization. *Nanoscale* **2014**, *6*, 1946–2008.

(18) Yu, J. C.; Yu; Ho; Jiang; Zhang. Effects of F- Doping on the Photocatalytic Activity and Microstructures of Nanocrystalline TiO_2 Powders. *Chem. Mater.* **2002**, *14*, 3808–3816.

(19) Livage, J.; Henry, M.; Sanchez, C. Sol-Gel Chemistry of Transition Metal Oxides. *Prog. Solid State Chem.* **1988**, *18*, 259–341.

(20) Kemnitz, E.; Groß, U.; Rüdiger, S.; Shekar, C. S. Amorphous Metal Fluorides with Extraordinary High Surface Areas. *Angew. Chem. Int. Ed.* **2003**, *42*, 4251–4254.

(21) Rüdiger, S.; Kemnitz, E. The Fluorolytic Sol–Gel Route to Metal Fluorides—a Versatile Process Opening a Variety of Application Fields. *Dalton Trans.* **2008**, 9, 1117–1127.

(22) Li, W.; Body, M.; Legein, C.; Borkiewicz, O. J.; Dambournet, D. Solvothermal Temperature Drives Morphological and Compositional Changes through Dehydroxyfluorination in Anatase Nanoparticles. *Eur. J. Inorg. Chem.* **2017**, *2017*, 192–197.

(23) Corradini, D.; Dambournet, D.; Salanne, M. Tuning the Electronic Structure of Anatase Through Fluorination. *Sci. Rep.* **2015**, *5*, 11553.

(24) Cava, R. J.; Murphy, D. W.; Zahurak, S.; Santoro, A.; Roth, R. S. The Crystal Structures of the Lithium-Inserted Metal Oxides $Li_{0.5}TiO_2$ Anatase, $LiTi_2O_4$ Spinel, and $Li_2Ti_2O_4$. *J. Solid State Chem.* **1984**, *53*, 64–75.

(25) Wagemaker, M.; Kearley, G. J.; van Well, A. A.; Mutka, H.; Mulder, F. M. Multiple Li Positions inside Oxygen Octahedra in Lithiated TiO_2 Anatase. *J. Am. Chem. Soc.* **2003**, *125*, 840–848.

(26) Wagemaker, M.; Borghols, W. J. H.; Mulder, F. M. Large Impact of Particle Size on Insertion Reactions. A Case for Anatase Li_xTiO_2. *J. Am. Chem. Soc.* **2007**, *129*, 4323–4327.

(27) Shen, K.; Chen, H.; Klaver, F.; Mulder, F. M.; Wagemaker, M. Impact of Particle Size on the Non-Equilibrium Phase Transition of Lithium-Inserted Anatase TiO_2. *Chem. Mater.* **2014**, *26*, 1608–1615.

(28) Morgan, B. J.; Watson, G. W. Role of Lithium Ordering in the Li_xTiO_2 Anatase → Titanate Phase Transition. *J. Phys. Chem. Lett.* **2011**, *2*, 1657–1661.

(29) Ma, J.; Li, W.; Morgan, B. J.; Światowska, J.; Baddour-Hadjean, R.; Body, M.; Legein, C.; Borkiewicz, O. J.; Leclerc, S.; Groult, H.; Lantelme, F.; Laberty-Robert, C.; Dambournet, D. Lithium Intercalation in Anatase Titanium Vacancies and the Role of Local Anionic Environment. *Chem. Mater.* **2018**, *30*, 3078–3089.

(30) Canepa, P.; Sai Gautam, G.; Hannah, D. C.; Malik, R.; Liu, M.; Gallagher, K. G.; Persson, K. A.; Ceder, G. Odyssey of Multivalent Cathode Materials: Open Questions and Future Challenges. *Chem. Rev.* **2017**, *117*, 4287–4341.

(31) Li, W.; Fukunishi, M.; Morgan, B. J.; Borkiewicz, O. J.; Pralong, V.; Maignan, A.; Groult, H.; Komaba, S.; Dambournet, D. The Electrochemical Storage Mechanism in Oxy-Hydroxyfluorinated Anatase for Sodium-Ion Batteries. *Inorg. Chem. Front.* **2018**, *5*, 1100–1106.

(32) Koketsu, T.; Ma, J.; Morgan, B. J.; Body, M.; Legein, C.; Goddard, P.; Borkiewicz, O. J.; Strasser, P.; Dambournet, D. Exploiting Cationic Vacancies for Increased Energy Densities in Dual-Ion Batteries. *Energy Storage Mater.* **2020**, *25*, 154–163.

(33) Ma, J.; Koketsu, T.; Morgan, B. J.; Legein, C.; Body, M.; Strasser, P.; Dambournet, D. Controlled Hydroxy-Fluorination Reaction of Anatase to Promote Mg^{2+} Mobility in Rechargeable Magnesium Batteries. *Chem. Commun.* **2018**, *54*, 10080–10083.

(34) Xia, Z.; Poeppelmeier, K. R. Chemistry-Inspired Adaptable Framework Structures. *Acc. Chem. Res.* **2017**, *50*, 1222–1230.

(35) Cooper, S. R.; Candler, R. O.; Cosby, A. G.; Johnson, D. W.; Jensen, K. M. Ø.; Hutchison, J. E. Evolution of Atomic-Level Structure in Sub-10 Nanometer Iron Oxide Nanocrystals: Influence on Cation Occupancy and Growth Rates. *ACS Nano* **2020**, *14*, 5480–5490.

(36) Haouari, C.; Squires, A. G.; Berthelot, R.; Stievano, L.; Sougrati, M. T.; Morgan, B. J.; Lebedev, O. I.; Iadecola, A.; Borkiewicz, O. J.; Dambournet, D. Impact of Solution Chemistry on Growth and Structural Features of Mo-Substituted Spinel Iron Oxides. *Inorg. Chem.* **2021**, *60*, 7217–7227.

(37) Gao, P.; Chen, Z.; Gong, Y.; Zhang, R.; Liu, H.; Tang, P.; Chen, X.; Passerini, S.; Liu, J. The Role of Cation Vacancies in Electrode Materials for Enhanced Electrochemical Energy Storage: Synthesis, Advanced Characterization, and Fundamentals. *Adv. Energy Mater.* **2020**, *10*, 1903780.

(38) Van der Ven, A.; Bhattacharya, J.; Belak, A. A. Understanding Li Diffusion in Li-Intercalation Compounds. *Acc. Chem. Res.* **2013**, *46*, 1216–1225.

(39) Gao, P.; Metz, P.; Hey, T.; Gong, Y.; Liu, D.; Edwards, D. D.; Howe, J. Y.; Huang, R.; Misture, S. T. The Critical Role of Point Defects in Improving the Specific Capacitance of δ-MnO_2 Nanosheets. *Nat. Commun.* **2017**, *8*, 14559.

(40) Koo, B.; Chattopadhyay, S.; Shibata, T.; Prakapenka, V. B.; Johnson, C. S.; Rajh, T.; Shevchenko, E. V. Intercalation of Sodium Ions into Hollow Iron Oxide Nanoparticles. *Chem. Mater.* **2013**, *25*, 245–252.

(41) Hahn, B. P.; Long, J. W.; Mansour, A. N.; Pettigrew, K. A.; Osofsky, M. S.; Rolison, D. R. Electrochemical Li-Ion Storage in Defect Spinel Iron Oxides: The Critical Role of Cation Vacancies. *Energy Environ. Sci.* **2011**, *4*, 1495–1502.

(42) Turner, S.; Buseck, P. R. Defects in Nsutite (γ-MnO_2) and Dry-Cell Battery Efficiency. *Nature* **1983**, *304*, 143–146.

(43) Sang, X.; Xie, Y.; Lin, M.-W.; Alhabeb, M.; Van Aken, K. L.; Gogotsi, Y.; Kent, P. R. C.; Xiao, K.; Unocic, R. R. Atomic Defects in Monolayer Titanium Carbide ($Ti_3C_2T_x$) MXene. *ACS Nano* **2016**, *10*, 9193–9200.

(44) Flambard, A.; Köhler, F. H.; Lescouëzec, R. Revisiting Prussian Blue Analogues with Solid-State MAS NMR Spectroscopy: Spin Density and Local Structure in $[Cd_3\{Fe(CN)_6\}_2]\cdot 15\ H_2O$. *Angew. Chem.* **2009**, *121*, 1701–1704.

(45) Simonov, A.; De Baerdemaeker, T.; Boström, H. L. B.; Ríos Gómez, M. L.; Gray, H. J.; Chernyshov, D.; Bosak, A.; Bürgi, H.-B.; Goodwin, A. L. Hidden Diversity of Vacancy Networks in Prussian Blue Analogues. *Nature* **2020**, *578*, 256–260.

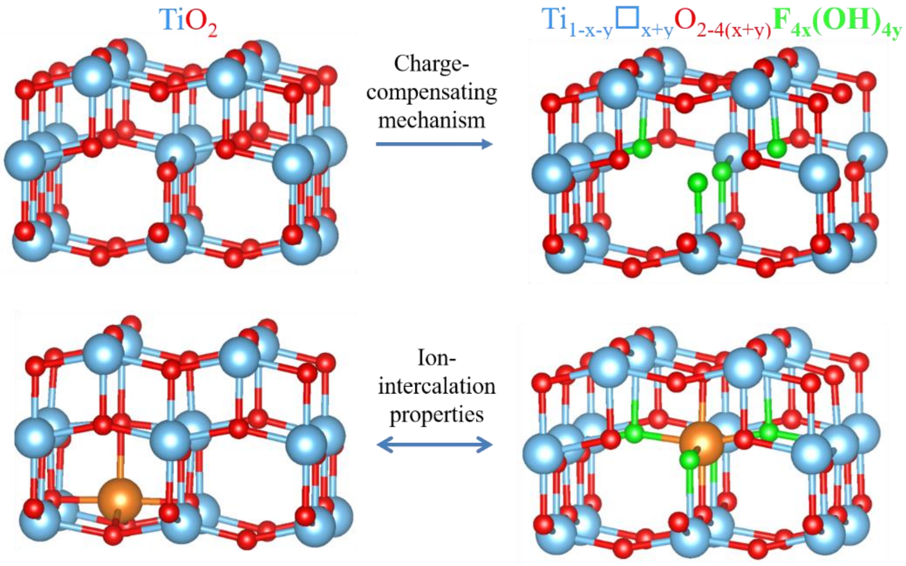
TiO_2
$Ti_{1-x-y}\square_{x+y}O_{2-4(x+y)}F_{4x}(OH)_{4y}$
Charge-compensating mechanism
Ion-intercalation properties